Near-infrared sensitivity enhancement of photorefractive polymer composites by pre-illumination

Mecher, Erwin; Gallego-Gómez, Francisco; Tillmann, Hartwig; Hörhold, Hans-Heinrich; Hummelen, Jan C.; Meerholz, Klaus; H. Horhold, H.

Published in:
Nature

DOI:
10.1038/nature00975

repetitive DNA conducts quite well[30]—both cases are in agreement with our model (Figs 2 and 3). Further, our results suggest that in non-repetitive long-range correlated regions of DNA, electrons can propagate over average distances of ~300 nucleotides, and that a fraction can propagate over distances of more than 1,000 nucleotides. In fact, the DNA segment in Fig. 4a, where our model predicts very good conducting behaviour, is even longer—extending to ~8,000 nucleotides. This conducting behaviour does not imply that correlated DNA is a macroscopic conductor, but rather that electronic transport at moderate distances can be found at $T = 0$. This distance range (~1 μm) is the focus of the above-mentioned experiments.

In summary, we find that long-range correlations change the localization properties of 1D disordered binary solids. We show that the localization length of the electron wavefunction is greatly increased by long-range correlations. In addition, for correlations stronger than a certain threshold, we find in the thermodynamic limit a broad energy band of extended states, and therefore a conducting phase. Thus, although still disordered, the 1D system can behave as a conductor, in contrast to the traditional theory which is applicable only for uncorrelated disorder. The threshold in the control parameter (the value of the correlation exponent) corresponds to a 'critical point' at which a metal–insulator transition takes place. These findings may be of importance for elucidating the electronic transport and the biological function of DNA segments with different types of correlations, as well as for the design of nanoscopic devices. □

Received 1 May; accepted 28 June 2002; doi:10.1038/nature00948.

1. Ashcroft, N. W. & Mermin, N. D. *Solid State Physics* (Holt-Saunders, London, 1976).
2. Anderson, P. W. Absence of diffusion in certain random lattices. *Phys. Rev.* **109,** 1492–1505 (1958).
3. Kramer, B. & MacKinnon, A. Localization: theory and experiment. *Rep. Prog. Phys.* **56,** 1469–1564 (1993).
4. Janssen, M. Statistics and scaling in disordered mesoscopic electron-systems. *Phys. Rep.* **295,** 1–91 (1998).
5. Peng, C.-K. *et al.* Long-range correlations in nucleotide sequences. *Nature* **356,** 168–170 (1992).
6. Holste, D., Grosse, I. & Herzel, H. Statistical analysis of the DNA sequence of human chromosome 22. *Phys. Rev. E* **64,** 041917 (2001).
7. Fink, H. V. & Schönenberger, C. Electrical conduction through DNA molecules. *Nature* **398,** 407–410 (1999).
8. Henderson, P. T., Jones, D., Hampikian, G., Kan, Y. & Schuster, G. B. Long distance charge transport in duplex DNA: The phonon-assisted polaron-like hopping mechanism. *Proc. Natl Acad. Sci. USA* **96,** 8353–8358 (1999).
9. Porath, D., Bezryadin, A., de Vries, S. & Dekker, C. Direct measurement of electrical transport through DNA molecules. *Nature* **403,** 635–638 (2000).
10. Hjort, M. & Stafstrom, S. Band resonant tunnelling in DNA molecules. *Phys. Rev. Lett.* **87,** 228101 (2001).
11. Mackinnon, A. & Kramer, B. One-parameter scaling of localization length and conductance in disordered systems. *Phys. Rev. Lett.* **47,** 1546–1549 (1981).
12. Hofstetter, E. & Schreiber, M. Statistical properties of the eigenvalue spectrum of the three-dimensional Anderson hamiltonian. *Phys. Rev. B* **48,** 16979–16985 (1993).
13. Kravchenko, S. V., Simonian, D., Sarachik, M. P., Mason, W. & Furneaux, J. E. Electric-field scaling at a B = 0 metal-insulator transition in 2 dimensions. *Phys. Rev. Lett.* **77,** 4398–4941 (1996).
14. Weymer, A. & Janssen, M. Localization length exponent, critical conductance distribution and mulifractality in hierarchical networks models for the quantum Hall-effect. *Ann. Phys. (Leipzig)* **7,** 159–173 (1998).
15. Schweitzer, L. & Zharekeshev, I. Kh. Scaling of level statistics and critical exponent of disordered 2-dimensional symplectic systems. *J. Phys. Condens. Matter* **9,** L441–L445 (1997).
16. Mott, N. F. & Twose, W. The theory of impurity conduction. *Adv. Phys.* **10,** 107–163 (1961).
17. Abou-Chacra, R., Anderson, P. W. & Thouless, D. J. A selfconsistent theory of localization. *J. Phys. C* **6,** 1734–1752 (1973).
18. Ishii, K. & Matsuda, H. Localization of normal modes and energy transport in the disordered harmonic chain. *Prog. Theor. Phys. Suppl.* **45,** 56–86 (1970).
19. Davids, P. S. Lyapunov exponents and transfer-matrix spectrum of the random binary alloy. *Phys. Rev. B* **52,** 4146–4155 (1995).
20. Dunlap, D. H., Wu, H.-L. & Phillips, P. Absence of localization in a random-dimer model. *Phys. Rev. Lett.* **65,** 88–91 (1990).
21. Phillips, P. & Wu, H.-L. Localization and its absence: a new metallic state for conducting polymers. *Science* **252,** 1805–1812 (1991).
22. de Moura, F. A. B. F. & Lyra, M. L. Delocalization in the 1D Anderson model with long-range correlated disorder. *Phys. Rev. Lett.* **81,** 3735–3738 (1998).
23. Kantelhardt, J. W., Russ, S., Bunde, A., Havlin, S. & Webman, I. Comment on delocalization in the 1 D Anderson model with long-range correlated disorder. *Phys. Rev. Lett.* **84,** 198–201 (2000).
24. Makse, H. A., Havlin, S., Schwartz, M. & Stanley, H. E. Method for generating long-range correlations for large systems. *Phys. Rev. E* **53,** 5445–5449 (1996).
25. Hu, K., Ivanov, P. Ch., Chen, Z., Carpena, P. & Stanley, H. E. Effect of trends on detrended fluctuation analysis. *Phys. Rev. E* **64,** 011114 (2001).
26. Chen, Z., Ivanov, P. Ch., Hu, K. & Stanley, H. E. Effect of nonstationarities on detrended fluctuation analysis. *Phys. Rev. E* **65,** 041107 (2002).
27. Dandliker, P. J., Holmlin, R. E. & Barton, J. K. Oxidative thymine dimer repair in the DNA helix. *Science* **275,** 1465–1468 (1997).
28. Kasumov, A. I. *et al.* Proximity-induced superconductivity in DNA. *Science* **291,** 280–282 (2001).
29. de Pablo, P. J. *et al.* Absence of dc-conductivity in λ-DNA. *Phys. Rev. Lett* **85,** 4992–4995 (2000).
30. Yoo, K.-H. *et al.* Electrical conduction through poly(dA)-poly(dT) and poly(dG)-poly(dC) DNA molecules. *Phys. Rev. Lett* **87,** 198102 (2001).

Supplementary information accompanies the paper on *Nature*'s website (http://www.nature.com/nature).

Acknowledgements

We thank L. Cruz for discussions, and the Spanish Ministerio de Educación y Cultura and NIH/National Center for Research Resources for support.

Competing interests statement

The authors declare that they have no competing financial interests.

Correspondence and requests for materials should be addressed to P.C. (e-mail: pcarpena@ctima.uma.es or pjcarpena@uma.es).

Near-infrared sensitivity enhancement of photorefractive polymer composites by pre-illumination

Erwin Mecher*, Francisco Gallego-Gómez*†, Hartwig Tillmann‡, Hans-Heinrich Hörhold‡, Jan C. Hummelen§ & Klaus Meerholz*†

* *Chemistry Department and Center for Nanoscience (CeNS), University of Munich, Butenandtstrasse 11, 81377 Munich, Germany*
‡ *Organic and Macromolecular Chemistry, University of Jena, Humboldtstrasse 10, 07743 Jena, Germany*
§ *Stratingh Institute and Materials Science Center, University of Groningen, Nijenborgh 4, 9747 AG Groningen, The Netherlands*

Among the various applications for reversible holographic storage media[1,2], a particularly interesting one is time-gated holographic imaging (TGHI)[3–5]. This technique could provide a noninvasive medical diagnosis tool, related to optical coherence tomography[6,7]. In this technique, biological samples are illuminated within their transparency window with near-infrared light, and information about subsurface features is obtained by a detection method that distinguishes between reflected photons originating from a certain depth and those scattered from various depths. Such an application requires reversible holographic storage media with very high sensitivity in the near-infrared. Photorefractive materials, in particular certain amorphous organic systems, are in principle promising candidate media, but their sensitivity has so far been too low, mainly owing to their long response times in the near-infrared. Here we introduce an organic photorefractive material—a composite based on the poly(arylene vinylene) copolymer TPD-PPV[8]—that exhibits favourable near-infrared characteristics. We show that pre-illumination of this material at a shorter wavelength before holographic recording improves the response time by a factor of 40. This process was found to be reversible. We demonstrate multiple holographic recording with this technique at video rate under practical conditions.

† Present address: Physical Chemistry Department, University of Cologne, Luxemburgerstrasse 116, 50939 Cologne, Germany.

Optical coherence tomography (OCT) has some shortcomings concerning the recording time, which could be overcome by using TGHI. The fundamental physical processes are identical for both techniques; the material is illuminated with low-coherence continuous-wave light or ultra-short laser pulses. Photons are mostly scattered, but a small percentage are reflected on material-characteristic features (so-called 'ballistic' photons). The scattered and reflected light is collected and fed into an interferometer (Michelson interferometer in OCT, holographic imaging system in TGHI). Because only the ballistic photons which come from a certain depth are coherent with the reference beam, an optical delay line can be used to determine the depth of the features to be recorded. The image contrast results from a combination of absorption and scattering features.

Photorefractive (PR) materials are well suited for TGHI, as the PR effect allows for recording holograms with high index modulation amplitudes even at low light levels owing to its time-integrating character. Also, the PR effect is reversible, that is, previously recorded holograms are erased or overwritten, a feature that would be mandatory for a commercial TGHI system. Photorefractivity requires photoconductivity and electro-optical response. In PR polymer composites these functions are achieved simply by mixing the appropriate functional components[9,10]. Most commonly, a sensitizer and nonlinear-optical chromophores are doped into a hole-conducting polymer host. To write a hologram the material is pre-poled by an external poling field E_0 and then illuminated by two coherent intersecting laser beams. In the bright regions of the resulting interference pattern absorption and field-enhanced exciton dissociation take place. The mobile charge carriers (mostly holes) are redistributed and become trapped in the dark regions, leading to an internal space-charge field E_{sc} (ref. 11). The superposition of E_0 and E_{sc} acts on the NLO chromophores, modulating the refractive index of the bulk to replicate the interference pattern[12,13].

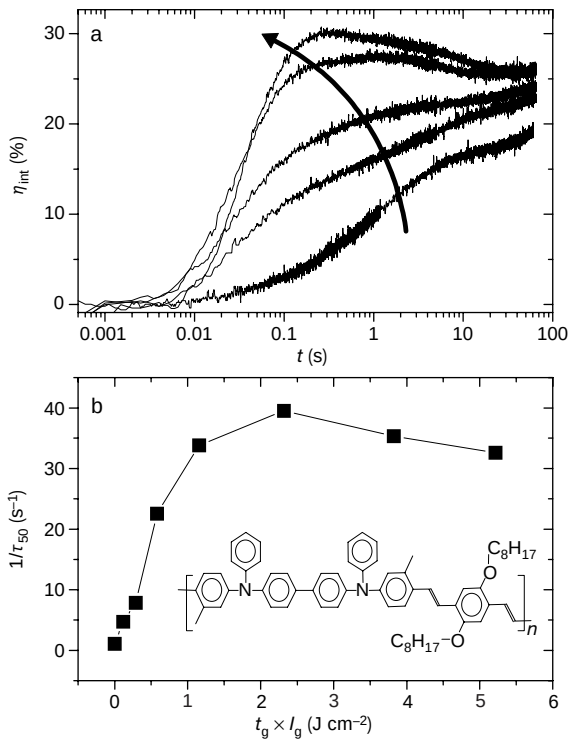

Figure 1 Holographic recording dynamics of the TPD-PPV-based composite for different gate intensities and chemical structure of TPD-PPV. **a**, Temporal evolution of the internal diffraction efficiency without gating (lowest curve) and after gate pulses with an intensity $I_g = 0.29$, 0.58, 2.3 and 5.2 W cm^{-2}, respectively. Total write-beam intensity $I_{WB,ext} = 3.27$ W cm^{-2}; gating time $t_g = 955$ ms; and external field $E_{ext} = 60$ V μm^{-1}. The arrow indicates increasing gate intensity. **b**, Dependence of the inverse response times τ_{50}^{-1} on the gating fluence. τ_{50} is the time necessary to reach 50% of the quasi-steady-state value of the diffraction efficiency (at 60 s). Inset, chemical structure of TPD-PPV.

A high sensitivity S is required to record a hologram with a sufficiently large external diffraction efficiency $\eta_{ext}(t_{exp})$ at low light levels (total external write-beam intensity $I_{WB,ext}$) and after a short exposure time t_{exp}. A technically widely used definition is[14] (see Methods):

$$S = \frac{\sqrt{\eta_{ext}(t_{exp})}}{I_{WB,ext} t_{exp}} \quad (1)$$

In organic PR materials a high sensitivity can be achieved by: (1) generating the highest possible PR space-charge field E_{SC}; (2) optimizing the EO chromophores[15]; (3) decreasing the absorption losses; and/or finally (4) decreasing the exposure time by increasing the recording speed. Here we report on the new photo-physical phenomenon of 'gating' in organic PR materials, which simultaneously tackles problems (1), (3) and (4) to yield unmatched near-infrared sensitivity in TPD-PPV-based PR devices.

$\eta_{ext}(t)$ was measured by four-wave mixing in a typical tilted geometry[9] with a wavelength of 830 nm (see Methods). The recording dynamics of the TPD-PPV-based material (see Methods for composition) was found to depend sublinearly on the recording intensity (not shown). This indicated that the grating build-up was limited by the generation of charge carriers.

Our method of speeding up the near-infrared recording process was specifically to pre-illuminate the material to provide carriers before the writing starts. Under these conditions the redistribution of the carriers (transport and trapping) might become the limiting step. Some attempts in this direction have already been reported in the literature: Silence *et al.*[16] found that pre-illumination irreversibly led to a slower response, but improved refractive index modulation amplitude Δn. The effect was referred to as 'optical trap activation'. Similarly, Herlocker *et al.* also reported a slowing of the response time owing to accumulation of traps[17]. Finally, Wolff *et al.* found no effect of pre-illumination on the recording process in their material[18]. Instead, when illuminated during recording the recording became faster, an effect referred to as 'optical trap filling'. Unfortunately, a strong loss in diffraction efficiency was anticipated. In our material, pre-illumination led to an acceleration of the recording process, unlike in all previous attempts. The pre-illumination effects were more pronounced when an independent light pulse of shorter wavelength was applied. In the context of this paper we refer to this procedure as 'gating', however, we point out that the mechanism discussed here is different from 'gating' in inorganic PR materials[19,20].

Figure 1a shows holographic recording traces for gating with $\lambda = 633$ nm light, using various intensities I_g and constant pulse duration t_g. A strong decrease of the response time by more than one order of magnitude and also a slight increase in η is observed.

Our explanation is the following. Gating leads to a spatially uniform distribution of charge carriers, which are absent in the pristine material (Fig. 2a). The carrier generation is much more efficient at shorter than at longer wavelengths, so gating is more efficient when short-wavelength light is used. The increase in η indicates that the number density of 'PR traps' N_t is increased by the pre-produced charges[16,21] and therefore E_{sc} can reach higher values. This interpretation is supported by measurements of the PR gain coefficient Γ, which was found to be larger in the non-illuminated (10 cm^{-1}) than in the gated samples (5 cm^{-1}) despite the increased Δn in the latter case, consistent with a higher trap density ($N_t \approx 2 \times 10^{17}$ cm^{-3} for gated compared with 10^{17} cm^{-3} for non-gated; see Methods). Beam coupling can lead to image distortions, so the

low gain coefficient found for this material is favourable for diffraction-based applications such as TGHI.

For high gating exposures intermediate diffraction maxima are observed in the temporal dependence (see Fig. 1a, top curve). Because temporal diffraction minima upon erasure are not observed, effects from competing hole and electron gratings as reported in ref. 22 can be excluded as an explanation. Instead, the occurrence of a temporal diffraction maximum indicates that E_{SC} is higher at intermediate times than in the quasi-steady state. This is the result of the advancing spatial charge separation (redistribution) on the one hand (higher E_{SC}) and a decreasing PR trap concentration caused by recombination on the other (lowering E_{SC}) as illustrated in Fig. 2b (time t_2).

The most prominent effect of the gating process is a strong increase of the recording speed. As a metric of comparison for the recording speed we plot $1/\tau_{50}$, the inverse of the time necessary to reach 50% of the quasi-steady-state value of the diffraction efficiency (Fig. 1b). Overall, the speed-up between gated and non-gated recording amounts to a factor of 40. This is an indication that indeed the carrier generation no longer limits the speed of the entire recording process. Instead the redistribution of carriers becomes the limiting process. This interpretation is supported by the finding that the gated recording speed at 830 nm is only about twice as slow as at a write wavelength of 633 nm, whereas the difference is much larger (by a factor of 80) for non-gated samples. In this context, we cannot distinguish whether or not the carrier mobility was affected by the gating.

The carrier distribution produced by the gating process is expected to relax over time due to recombination. To verify this a temporal delay t_d was introduced between applying the gate beam and starting the writing process. We found that the recording slows down exponentially, reaching a relaxed state (equal to non-gated samples) after $t_d \approx 50$ s. From this we conclude that the recording speed correlates with density of pre-existing charge carriers.

With increasing gate fluence, the number density of free charge carriers will pass through a maximum that is due to trapping, which explains the reduction in recording speed for high pre-exposure doses (Fig. 1b). Because we observe faster recording speed by pre-illumination as well as by illumination during recording, unlike Wolff *et al.*[18], this indicates that the carriers remain 'free' for a rather long time. These considerations are backed by transient measurements of the photocurrent using experimental conditions similar to those used here (L. Kulikovsky, E.M., K.M. and D. Neher, manuscript in preparation) and are further supported by redox-chemical

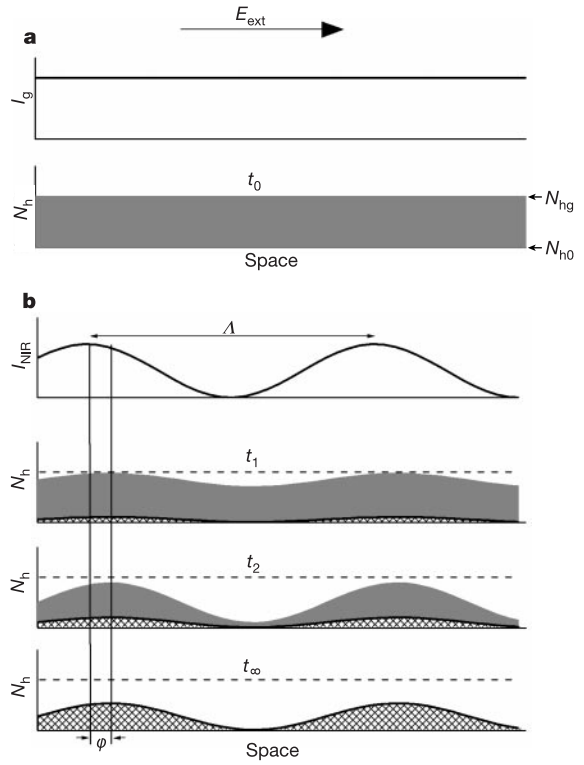

Figure 2 Illustration of the gating mechanism. **a**, A pristine sample exhibits a vanishing, spatially uniform charge carrier distribution N_0. Uniform pre-illumination with a gate beam of intensity I_g (top) increases the carrier density to N_g (bottom). For reasons of electroneutrality, the number densities of holes and electrons are equal. In TPD-PPV holes are much more mobile than electrons, so we show the distribution N_h of holes only. **b**, During the writing procedure the interference pattern with the intensity I_{NIR} (top, grating period Λ) spatially modulates the hole density N_h. Snapshots of the situation before steady state is reached are shown for two write times $t_1 < t_2$ (upper/lower middle) and the quasi-steady-state value t_∞ (bottom). Without gating free holes are generated in the bright regions and redistributed (black cross-hatched area). The modulation amplitude increases monotonously in time and finally reaches the quasi-steady-state value at t_∞. The recording process is relatively slow. By contrast, with gating the modulation (grey filled area) is 'carved' in the initial hole density (dashed line). At intermediate times (t_2) the modulation can assume larger values than in the quasi-steady-state value (t_∞), which is identical to the case without gating. The gated recording process is relatively fast. For simplicity, this illustration assumes a constant spatial relocation φ of the carriers relative to the incident interference pattern.

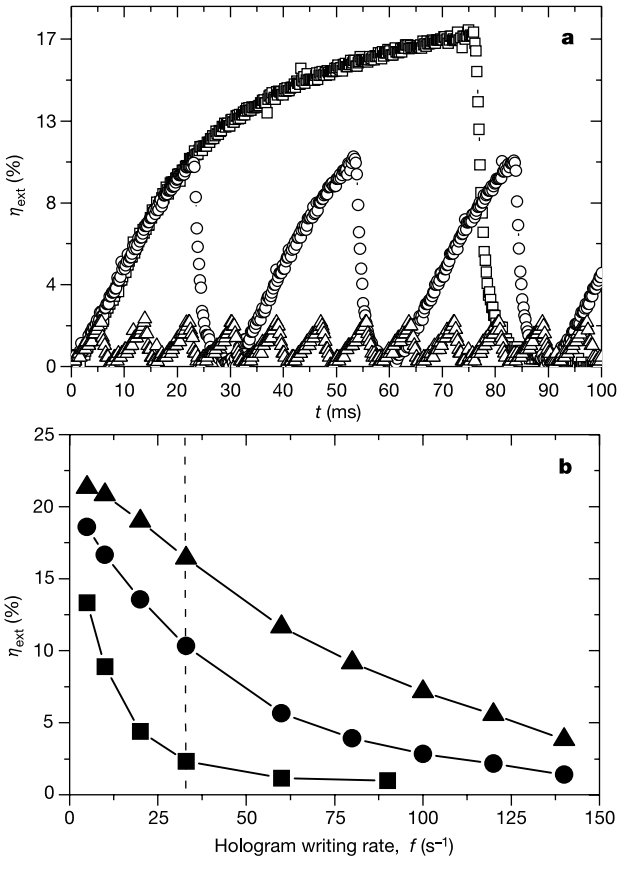

Figure 3 Gated holographic recording dynamics of the TPD-PPV-based composite for different write rates and write intensities. **a**, Time dependence of the external diffraction efficiency for a hologram write rate of 10 Hz (squares), 33 Hz (circles) and 120 Hz (triangles), respectively. $I_{WB,ext} = 3.27\,W\,cm^{-2}$, $I_g = 2\,W\,cm^{-2}$, $E_{ext} = 60\,V\,\mu m^{-1}$. **b**, End values of the external diffraction efficiencies achieved at different hologram write rates with $I_{WB,ext} = 0.65$ (squares), 3.27 (circles) and 6.54 $W\,cm^{-2}$ (triangles), respectively. $I_g = 2\,W\,cm^{-2}$, $E_{ext} = 60\,V\,\mu m^{-1}$. Solid lines are guides to the eye. The dashed line marks the video-rate frequency.

doping (oxidation) of the material, providing permanent traps in the material. This allowed us to achieve part of the sensitivity enhancement even without pre-illumination (E.M. and K.M., manuscript in preparation).

We checked whether the new gating effect is a unique property of the TPD-PPV-based material used here or whether it can be observed in composites based on the commonly used hole-conducting matrix poly(*N*-vinylcarbazole) (PVK) using the same azo dyes as electro-optical components. When sensitized with 2,4,7-trinitrofluorenone (TNF) or the C_{60} derivative PCBM (see Methods) the gating effect was present. No gating effects were found in PVK-based materials sensitized with 2,4,7-trinitrofluorenonemalononitrile (TNFM), the sensitizer usually employed for carbazole-containing hole-conductors in the near-infrared region (E.M. and K.M., manuscript in preparation).

To demonstrate the high sensitivity of our new material, we performed a pulsed recording experiment. During the first three quarters of a recording cycle both write beams were on and the gate beam was off, and vice versa during the last quarter. Thus, the gate beam also serves efficiently to erase the previously written hologram. During each cycle a hologram with an external diffraction efficiency of several per cent can be written and be completely erased (Fig. 3a). This experiment was performed for different hologram write rates and different write beam intensities (Fig. 3b). At a write rate of 90 Hz and a write beam intensity of $I_{WB,ext} = 0.64\,W\,cm^{-2}$ ($I_{WB,int} = 0.2\,W\,cm^{-2}$), a value of $\eta_{ext} \approx 1\%$ was still achieved, yielding a sensitivity of $19\,cm^2\,J^{-1}$. No long-term changes of the PR performance under permanent use (overnight video-rate experiment corresponding to about 1.2 million completed exposure and erasure cycles) were observed.

Our devices are about one order of magnitude more sensitive at a given external field than the previously best organic PR devices: a multifunctional glass[23] and a methine dye[24] (Table 1). The latter were about twice as sensitive as the best PVK/TNFM-based systems[25,26]. The PVK/TNFM-based composite investigated here (Table 1) had reduced sensitivity by even more than two orders of magnitude. We point out that a true comparison is difficult, because of differences in the experimental conditions employed by the different groups, such as device thickness, operating wavelength and the electric field strength.

Inorganic materials such as multiple quantum wells[4] and Rh-doped $BaTiO_3$ crystals[3] have been used for TGHI in the near-infrared. Multiple quantum wells operate in the thin-grating limit ($d \approx 1\,\mu m$; Raman–Nath regime), whereas the PR crystals are rather thick recording media (d is several mm; Bragg regime). Despite their relatively small active-layer thickness ($d \approx 100\,\mu m$) high-performance PR polymer devices show much higher diffraction efficiencies than the inorganic materials. Their response time is slower than in multiple quantum well devices ($\tau < 1$ ms), but faster than in Rh-$BaTiO_3$ ($\tau \approx 1$ s; ref. 3). Overall, the sensitivity (equation (1)) of organic PR devices is higher than in the inorganic counterparts. Furthermore, they offer the important advantage of a large aperture. This permits holographic recording with high spatial resolution (diffraction limited, that is, 3 μm in our case) and high angular bandwidth[5].

The characterization presented so far was performed under 'ideal' (laboratory) conditions, that is, with plane-wave write beams, rather high intensity, and with high fringe contrast m (≈1). Under 'real' conditions much diffraction efficiency is lost because the object wave is distorted and usually much weaker than the reference wave, yielding poor contrast m. To demonstrate that our devices can still perform under these conditions, we set up a video-rate (30 Hz) imaging holographic system. Considering the low total intensity, the unfavourable write beam intensity ratio (~15) and the rather strong readout beam (yielding $m \approx 0.4$; see Methods for details), a respectable overall diffraction efficiency of the entire setup of 10^{-3} (at $E_{ext} = 60\,V\,\mu m^{-1}$) was nevertheless measured at the image output plane, allowing readout with a low-cost charge-coupled device (CCD) camera. In our case, the strong readout beam mimics the high background given by the diffusely scattered photons in a TGHI experiment. In a real application readout would be performed with a short pulse at the end of the write phase and not continuously.

The degree of scattering as well as the required resolution in the biological specimen will eventually determine the depth up to which OCT and TGHI can be used. Typical values range from 0.5 mm to 2 mm (ref. 6). If the ballistic photons are a fraction of 10^{-4} of the total photons (that is, 99.99% scatter) the contrast factor would be $m \approx 0.01$, a reduction of m by a factor of about 40 compared with our video-rate experiment (see above). According to equations (3) to (5) (see 'parameter determination' section) this would reduce the diffraction efficiency by a factor of 40^2, yielding an overall $\eta \approx 10^{-6}$ assuming constant recording speed (E.M. and K.M., manuscript in preparation). The reduction in signal can be at least partially compensated for by using more sensitive CCD detectors.

In both OCT and TGHI, the depth resolution (z-direction) is given by the bandwidth of the low-coherence light source[6,7]. It is 10–15 μm in commercial OCT systems using normal super-luminescence diodes. Up to 1–3 μm resolution has been achieved by ultra-short laser pulses[7]. For OCT the lateral resolution (x–y plane) is given by the spacing between adjacent scan points, whereas TGHI provides diffraction-limited x–y resolution (3 μm in the geometry

Table 1 **Near-infrared sensitivity comparison of selected organic photorefractive materials**

Material composition (wt%)	Wavelength of write beam, λ_{WB} (nm)	Intensity of write beam, I_{WB} ($W\,cm^{-2}$)	External field, E_{ext} ($V\,\mu m^{-1}$)	Exposure time, t_{exp} (s)	Sensitivity, S ($cm^2\,J^{-1}$)	S rescaled to $60\,V\,\mu m^{-1}$ ($cm^2\,J^{-1}$)†	Ref.
AZO:TPD-PPV:DPP:PCBM 30:56:13:1, gated at 633 nm ($2\,W\,cm^{-2}$)	830	0.65	60	0.008	19	19	This work
DRDCTA:EHMPA:TNFM 69:30:1	790	1	80	~0.013	7.7	~3.2	23
Methin dye 100	780	3	84	~0.005*	6.7	~2.4	24
Chrom. C:PVK:ECZ:TNFM 28.5:45:25.5:1	780	5	48	0.03	0.67	~1.3	25
DHAC-MPN:PVK:DPP:TNFM 25:49:24:2	830	1	29	0.8	0.13	~1.1	26
AZO:PVK:ECZ:TNFM 30:46:23:1	830	3.27	60	0.37	0.08	0.08	This work

*Estimated from fit parameters given in ref. 24.
†The sensitivity is strongly field dependent. For comparing the devices we tried to rescale the sensitivities to a field to $60\,V\,cm^{-1}$ by assuming $\sqrt{\eta_{ext}} \propto E_{ext}^2$ (typically observed in low-T_g materials[12,13]) and $t_{exp} \propto E_{ext}^{-1}$. We point out that this procedure tends to underestimate (overestimate) S for upscaling (downscaling) because the field dependence of the recording time of real system is generally stronger than linear (for example, ref. 23).
AZO, azo dye mixture described in Methods.

used here) owing to the parallel imaging character of holography. Thus, in TGHI the processing time is independent of the *x*–*y* image size, but in OCT this scales with the area and the lateral resolution, that is, with the total number of data points to be scanned. For comparison, OCT systems require about 10 s for recording one *x*–*y* image plane of $1.5 \times 2\,mm^2$ with 5 μm resolution[27]. By using an exposure time longer than 33 ms for the material presented here we could regain diffraction efficiency and still achieve a more favourable recording rate in a TGHI system.

Whereas achieving high refractive index modulation amplitudes with optimized nonlinear-optical chromophores is well understood[15], this work opens the way for achieving high recording speeds. Now, sufficiently large external diffraction efficiencies are feasible without sacrificing speed. Gating may make it possible to extend the operation wavelength of organic PR materials further towards the infrared.

We have demonstrated multiple-video-rate holographic storage with low light power and moderate field strength using a real object. Similar experiments using near-infrared laser light were not previously possible. The availability of low-cost, high-power NIR laser diodes and sensitive CCD chips make the development of an operating time-gated holographic imaging system seem economically feasible. TGHI promises faster recording time than commercial OCT, particularly for large regions of interest. One benefit would be a reduced tendency towards 'motion artefacts' which are often anticipated in *in vivo* studies by OCT. □

Methods

Material composition

The material investigated was based on TPD-PPV (56 wt%, chemical structure shown in Fig. 1b) as the photoconductive host matrix. The eutectic mixture of two azo dyes (2,5-dimethyl-(4-*p*-nitrophenylazo)-anisole and 3-methoxy-(4-*p*-nitrophenylazo)-anisole, ratio 1:1; 30 wt%) was used as the electro-optical component. Diphenyl-phthalate (DPP, 13 wt%) was used as a plasticizer to ensure sufficient orientational mobility for the chromophores. Finally, as the sensitizer, 1 wt% of the highly soluble C_{60} derivative [6,6]-phenyl-C61-butyricacid-methylester (PCBM) was added[28]. The resulting composite had a glass transition temperature $T_g \approx 10\,°C$ (differential scanning calorimetry, heating rate + 20 K min^{-1}); measurements were made at 22 °C. The absorption coefficients at 830 (633) nm were 5 (155) cm^{-1}.

Holographic set-up parameters

Holographic experiments were performed (40-mW laser diode) with two s-polarized write beams (1 and 2) with external angles $\alpha_{1,ext} = 50.8°$ and $\alpha_{2,ext} = 71.1°$ relative to the sample normal. The write beams were overlapped in 105-μm-thick polymer films sandwiched between ITO/glass electrodes. The full-width at half-maximum (FWHM) of the plane gaussian writing beams was 0.47 mm. Owing to the tilted geometry, the illuminated area is elliptical with a half-maximum surface of 0.273 mm^2 (0.535 mm^2) for write beam 1 (2). Reflection losses in the multilayer device before entering the composite were calculated to be 13% (33%) for write beam 1 (2). 1 W cm^{-2} internal intensity corresponds to a external intensity of 3.27 W cm^{-2}. The external diffraction efficiency η_{ext} was determined in degenerate four-wave mixing experiments. Readout was performed by a weak p-polarized probe beam (external intensity $I_{R,ext}$, diffracted component $I_{R,diffr}$) counter-propagating to beam 1.

Parameter determination

η_{ext} was calculated according to

$$\eta_{ext} = I_{R,diff}/I_{R,ext} \tag{2}$$

η_{ext} depends on the refractive index modulation amplitude Δn according to

$$\eta_{ext} = R\exp(-\alpha d/\cos\alpha_1)\eta_{int} \tag{3a}$$

$$\eta_{int} = \sin^2\left(\frac{\pi\Delta n d}{\lambda\cos\alpha_1}\right) \tag{3b}$$

Here η_{int} is the internal diffraction efficiency, α is the absorption coefficient, d is the sample thickness, λ is the laser wavelength, α_1 is the internal angle of the read beam relative to the sample normal, and $R < 1$ is a factor taking into account reflection losses. Δn is given by

$$\Delta n \approx E_0 E_{SC} r_{EO,eff} \tag{4}$$

$r_{EO,eff}$ is the effective electro-optical coefficient, which by itself depends on number density of EO chromophores and the PR molecular figure-of-merit (FOM) of the chromophore[13]. E_{sc} is the space-charge field, which is proportional[11] to the contrast factor m of the grating given by

$$m = 2(I_1 I_2)^{1/2}/I_{tot} \tag{5}$$

where I_{tot} is the total light intensity incident on the device, including read beam and incoherent illumination (scattered light in TGHI). For the systematic studies the external write-beam powers were adjusted such that the internal intensities were equal, that is, $m \approx 1$ owing to the weak read beam intensity.

The field-dependent two-beam coupling gain coefficient $\Gamma(E)$, which describes the energy transfer between the write beams, was calculated from the transmitted write-beam intensities I_1 and I_2 according to

$$\Gamma = \frac{1}{d}\left[\cos a_1 \ln\frac{I_1(E)}{I_1(E=0)} - \cos a_2 \ln\frac{I_2(E)}{I_2(E=0)}\right] \tag{6}$$

According to ref. 9 Γ can be approximated by

$$\Gamma \approx C_{TBC}\Delta n \sin(\varphi_g) \tag{7}$$

with $C_{TBC} = 2\pi/\{\lambda_0 \cos[(\alpha_2 - \alpha_1)/2]\}$, φ_g is the phase shift between the light interference pattern and the PR index grating. The trap density N_T was calculated from Δn and Γ according to the standard Kukhtarev model developed for inorganic PR crystals[11].

As a metric of comparison and to qualitatively visualize the influence that the gating has on the recording dynamics, we use the time to reach 50% of the quasi-steady-state diffraction efficiency after 60 s of recording, τ_{50}.

Recording scheme

The recording dynamics without gating was determined by switching both write beams on after a pre-poling period in the dark $t_p = 300$ s (much longer than the relaxation time; see main text) and monitoring of $I_{R,diffr}$. For the gating experiments a gate pulse from a 633-nm HeNe-laser with duration t_g and intensity I_g was applied at normal incidence during the pre-poling period right before switching on the near-infrared write beams.

Holographic imaging set-up

The video-rate holographic imaging set-up contained a moving slide ($1 \times 2\,mm^2$ object size) as the input mask. Read-out was performed with the back-reflected reference wave after rotating its polarization by 90° to p-polarization. The total external powers of the 830 nm write and read beams (FWHM, 1.3 mm) were $P_{obj} = 0.4$ mW, $P_{ref} = 5.8$ mW, $P_{read} = 1.8$ mW; gating was performed at 633 nm with $P_{gate} = 8$ mW (FWHM, 1.3 mm). According to equation (5) the average grating contrast was $m \approx 0.4$.

Received 31 October 2001; accepted 8 July 2002; doi:10.1038/nature00975.

1. Burr, G. W. & Leyva, I. Multiplexed phase-conjugate holographic data storage with a buffer hologram. *Opt. Lett.* **25,** 499–501 (2000).
2. Stepanov, S. in *Handbook of Advanced Electronic and Photonic Materials and Devices* Ch. 6 (ed. Nalva, H. S.) Vol. 2 (Academic, New York, 2001).
3. Hyde, S. C. W. *et al.* Depth-resolved holographic imaging through scattering media by photorefraction. *Opt. Lett.* **20,** 1331–1334 (1995).
4. Jones, R. *et al.* Holographic storage and high background imaging using photorefractive multiple quantum wells. *Appl. Phys. Lett.* **69,** 1837–1839 (1996).
5. Steele, D. D. *et al.* Transillumination imaging through scattering media by use of photorefractive polymers. *Opt. Lett.* **23,** 153–155 (1998).
6. Huang, D. *et al.* Optical coherence tomography. *Science* **254,** 1178–1181 (1991).
7. Drexler, W. *et al. In vivo* ultrahigh-resolution optical coherence tomography. *Opt. Lett.* **24,** 1221–1123 (1999).
8. Hörhold, H. H. *et al.* Synthesis of TPD-containing polymers for use as light-emitting materials in electroluminescent and laser devices. *Proc. SPIE* **4105,** 431–442 (2001).
9. Moerner, W. E., Grunnet-Jepsen, A. & Thompson, C. L. Photorefractive polymers. *Annu. Rev. Mater. Sci.* **27,** 585–623 (1997).
10. Zilker, S. Materials design and physics of organic photorefractive systems. *ChemPhysChem* **1,** 72–87 (2000).
11. Kukhtarev, N. V., Markov, V. B., Odulov, S. G., Soskin, M. S. & Vinetskii, V. L. Holographic storage in electrooptic crystals. I. Steady state. *Ferroelectrics* **22,** 949–960 (1979).
12. Moerner, W. E., Silence, S. M., Hache, F. & Bjorklund, G. C. Orientationally enhanced photorefractive effect in polymers. *J. Opt. Soc. Am.* **11,** 320–330 (1994).
13. Wortmann, R. *et al.* Design of optimized photorefractive polymers: A novel class of chromophores. *J. Chem. Phys.* **105,** 10637–10647 (1996).
14. Ashley, J. *et al.* Holographic data storage. *IBM J. Res. Dev.* **44,** 341–367 (2000).
15. Würthner, F., Wortmann, R. & Meerholz, K. Chromophore design for photorefractive organic materials. *ChemPhysChem* **3,** 17–31 (2002).
16. Silence, S. M., Bjorklund, G. C. & Moerner, W. E. Optical trap activation in a photorefractive polymer. *Opt. Lett.* **19,** 1822–1824 (1994).
17. Herlocker, J. A. *et al.* Stabilization of the response time in photorefractive polymers. *Appl. Phys. Lett.* **77,** 2292–2294 (2000).
18. Wolff, J., Schloter, S., Hofmann, U., Haarer, D. & Zilker, S. Speed enhancement of photorefractive polymers by means of light-induced filling of trapping states. *J. Opt. Soc. Am. B* **16,** 1080–1086 (1999).
19. Buse, K., Adibi, A. & Psaltis, D. Non-volatile holographic storage in doubly doped lithium niobate crystals. *Nature* **393,** 665–668 (1998).
20. Günther, H., Macfarlane, R., Furukawa, Y., Kitamura, K. & Neurgaonkar, R. Two-color holography in reduced near-stoichiometric lithium niobate. *Appl. Opt.* **73,** 7611–7623 (1998).
21. Grunnet-Jepsen, A. Spectroscopic determination of trap density in C60-sensitized photorefractive polymers. *Chem. Phys. Lett.* **291,** 553–561 (1998).
22. Wang, L., Ng, M.-K. & Yu, L. Photorefraction and complementary grating competition in bipolar transport molecular material. *Phys. Rev. B.* **62,** 4973–4984 (2000).
23. Zilker, S. J. & Hofmann, U. Organic photorefractive glass with infrared sensitivity and fast response. *Appl. Opt.* **39,** 2287–2290 (2000).
24. Wang, L., Ng, M. K. & Yu, L. Efficient molecular photorefractive materials based on methine dyes. *Appl. Phys. Lett.* **78,** 700–702 (2001).
25. Steenwinckel, D. V., Hendrickx, E., Persoons, A., Van den Broeck, K. & Samyn, C. Influence of the

chromophore ionization potential on speed and magnitude of photorefractive effects in poly-N-vinylcarbazole based polymer composites. *J. Chem. Phys.* **112,** 11030–11037 (2000).
26. Kippelen, B. *et al.* Infrared photorefractive polymers and their applications for imaging. *Science* **279,** 54–57 (1998).
27. Boppart, S. A. *et al. In vivo* cellular optical coherence tomography imaging. *Nature Med.* **4,** 861–865 (1998).
28. Hummelen, J. C. *et al.* Preparation and characterization of fulleroid and methanofullerene derivatives. *J. Org. Chem.* **60,** 532–538 (1995).

Acknowledgements

We thank R. Bittner, D. Müller, M. Hofmann and R. Birngruber for discussions. Financial support was granted by the Volkswagen Foundation (Germany), the European Space Agency (MAP-project), the Fonds der Chemischen Industrie (Germany), and the Bavarian government through 'Neue Werkstoffe' (Germany).

Competing interests statement

The authors declare that they have no competing financial interests.

Correspondence and requests for materials should be addressed to K.M. (e-mail: klaus.meerholz@uni-koeln.de).

Hydrogen from catalytic reforming of biomass-derived hydrocarbons in liquid water

R. D. Cortright, R. R. Davda & J. A. Dumesic

Department of Chemical Engineering, University of Wisconsin, Madison, Wisconsin 53706, USA

Concerns about the depletion of fossil fuel reserves and the pollution caused by continuously increasing energy demands make hydrogen an attractive alternative energy source. Hydrogen is currently derived from nonrenewable natural gas and petroleum[1], but could in principle be generated from renewable resources such as biomass or water. However, efficient hydrogen production from water remains difficult and technologies for generating hydrogen from biomass, such as enzymatic decomposition of sugars[2–5], steam-reforming of bio-oils[6–8] and gasification[9], suffer from low hydrogen production rates and/or complex processing requirements. Here we demonstrate that hydrogen can be produced from sugars and alcohols at temperatures near 500 K in a single-reactor aqueous-phase reforming process using a platinum-based catalyst. We are able to convert glucose—which makes up the major energy reserves in plants and animals—to hydrogen and gaseous alkanes, with hydrogen constituting 50% of the products. We find that the selectivity for hydrogen production increases when we use molecules that are more reduced than sugars, with ethylene glycol and methanol being almost completely converted into hydrogen and carbon dioxide. These findings suggest that catalytic aqueous-phase reforming might prove useful for the generation of hydrogen-rich fuel gas from carbohydrates extracted from renewable biomass and biomass waste streams.

We consider production of hydrogen by low-temperature reforming (at 500 K) of oxygenated hydrocarbons having a C:O stoichiometry of 1:1. For example, reforming of the sugar–alcohol sorbitol to H_2 and CO_2 occurs according to the following stoichiometric reaction:

$$C_6O_6H_{14}(l) + 6H_2O(l) \rightleftharpoons 13H_2(g) + 6CO_2(g) \quad (1)$$

The equilibrium constant for reaction (1) per mole of CO_2 is of the order of 10^8 at 500 K, indicating that the conversion of sorbitol in the presence of water to H_2 and CO_2 is highly favourable. However, the selective generation of hydrogen by this route is difficult because the products H_2 and CO_2 readily react at low temperatures to form alkanes and water. For example, the equilibrium constant at 500 K for the conversion of CO_2 and H_2 to methane (reaction 2) is of the order of 10^{10} per mole of CO_2.

$$CO_2(g) + 4H_2(g) \rightleftharpoons CH_4(g) + 2H_2O(g) \quad (2)$$

Figure 1 shows a schematic representation of the reaction pathways we believe to be involved in the formation of H_2 and alkanes from oxygenated hydrocarbons over a metal catalyst. The reactant undergoes dehydrogenation steps on the metal surface to give adsorbed intermediates before the cleavage of C–C or C–O bonds. With platinum, the catalyst we use, the activation energy barriers for cleavage of O–H and C–H bonds are similar[10]; however, Pt–C bonds are more stable than Pt–O bonds, so adsorbed species are probably bonded preferentially to the catalyst surface through Pt–C bonds. Subsequent cleavage of C–C bonds leads to the formation of CO and H_2, and CO reacts with water to form CO_2 and H_2 by the water–gas shift reaction (that is, $CO + H_2O \rightleftharpoons CO_2 + H_2$)[11,12].

The further reaction of CO and/or CO_2 with H_2 leads to alkanes and water by methanation and Fischer–Tropsch reactions[13–15]; this H_2 consuming reaction thus represents a series-selectivity challenge. In addition, undesirable alkanes can form on the catalyst surface by cleavage of C–O bonds, followed by hydrogenation of the resulting adsorbed species. This process constitutes a parallel-selectivity challenge. Another pathway that contributes to this parallel-selectivity challenge is cleavage of C–O bonds through dehydration reactions catalysed by acidic sites associated with the catalyst support[16,17] or catalysed by protons in the aqueous solution[18,19], followed by hydrogenation reactions on the catalyst. In addition, organic acids can be formed by dehydrogenation reactions catalysed by the metal, followed by rearrangement reactions[20] that take place in solution or on the catalyst. These organic acids lead to the formation of alkanes from carbon atoms that are not bonded to oxygen atoms.

Table 1 summarizes our experimental results for aqueous-phase reforming of glucose, the compound most relevant to hydrogen production from biomass, as well as for the reforming of sorbitol, glycerol, ethylene glycol and methanol. Reactions were carried out over a Pt/Al_2O_3 catalyst at 498 and 538 K (see Methods for experimental details). The fractions of the feed carbon detected in the effluent gas and liquid streams yield a complete carbon balance for all feed molecules, indicating that negligible amounts of carbon have been deposited on the catalyst. Catalyst performance was stable

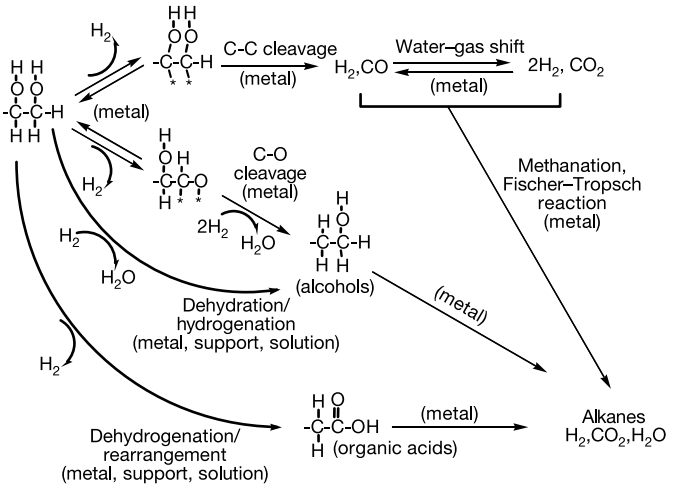

Figure 1 Reaction pathways for production of H_2 by reactions of oxygenated hydrocarbons with water. (Asterisk represents a surface metal site.)

